

Measuring different types of Cepheid Variables

Physics Department, University of California, Santa Barbara, CA 93106

(Data: submitted June 3, 2022)

In this paper, I used a 0.4 meter telescope to observe three Cepheid variables. The three Cepheid variables each belong to a specific type of Cepheid variables, which are classical Cepheid variables, type II Cepheid variables, and RR type Cepheid variables. Photos of the three Cepheid variables are taken using telescope. Photometry techniques are conducted to obtain the luminosity-period relation of the Cepheid variables

PACS коды:

I. BACKGROUND

A Cepheid variable is a type of star that varies in both diameter and temperature, resulting changes in brightness. The variation of Cepheid variables is highly predictable. The period of the Cepheid variables is directly related to their absolute magnitude. They change their brightness in a well-defined stable period and amplitude. Almost every Cepheid variables follow this relation extremely well. [3] The characteristic of Cepheids was first discovered in 1908 by Henrietta Swan Leavitt after studying thousands of variable stars in the Magellan Clouds.[2] The name, Cepheid, comes from Delta Cephei in the constellation Cepheus, which is the first star to be identified as this kind variables. The strong direct relation between the Cepheid variable's luminosity and pulsation period established Cepheids as important indicators in the distance measurement in astronomy. Once the period of a Cepheid variable is measured, its absolute magnitude can be inferred from the luminosity-period relation. Compare the absolute magnitude and the apparent magnitude, the distance to the Cepheid variable can be obtain. The distance measurement by Cepheid variables can be used to measure extremely large distance, such as the distance between the Milky way and another galaxy. Astronomer Edwin Hubble used Cepheid variable for the first time to measure the distance between the Earth and the Andromeda Galaxy. The result is far greater than the diameter of the Milky way. Thus, he determined that Andromeda is not located in the Milky way. There are many galaxies existing out of the Milky way.[4]. The mechanism of the varying nature of the Cepheid variables was understood as star heat engine proposed by Arthur Stanley Eddington in 1917.[9] The mechanism was further explained by S.A. Zhevakin in 1957, who identified ionized helium as a likely valve for the engine. [10]

II. APPROACH

A. objects choosing

three Cepheid variables, each belong to a specific type of Cepheid variables, which are classical Cepheid variables, type II Cepheid variables, and RR type Cepheid variables, were chosen. RR lyrae, NSV 4148, and BI Cas were chosen

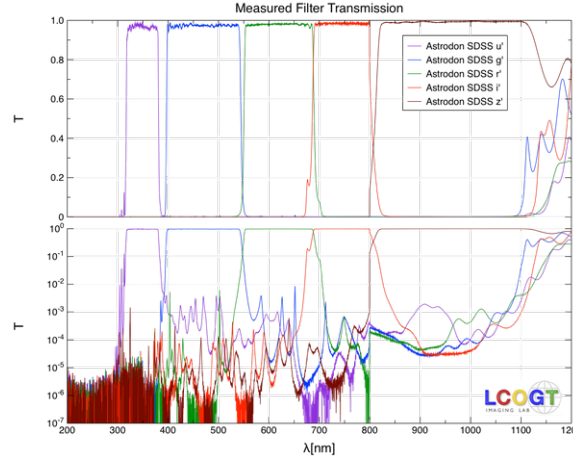


Рис. 1: The transmission data of SDSS u' , SDSS g' , SDSS r' , and SDSS i' filters.[7]

as observation target. RR lyrae is classified as anomalous Cepheid variables, or more specifically, RR lyrae variables. Since RR lyrae is the most iconic one among this type. NSV 4148 is classified as classical Cepheid variables while BI Cas is classified as type II Cepheid variables.[1]. According to the variable data base, NSV 4148 has a mean apparent magnitude of 11.79, period 0.894 day. BI Cas has a mean apparent magnitude of 12.8, period 1.099 days. And RR lyrae has a mean apparent magnitude of 8.55, period 0.567 day.

B. observing instruments and parameters

In this paper, a 0.4 meter telescope from the Las Cumbres Observatory was used to take photos of the Cepheid variables. The telescope has a FOV of 29.2×19.5 in arc min. The instrument on the telescope is SBIG STL6303 camera, which has a pixel size of 0.571 arc sec and 2048×3072 pixels in total. Further information about the instruments used can be found in the reference.[5] Exposure time is calculated using LCO exposure time calculator.[6] SDSS u' , SDSS g' , SDSS r' , and SDSS i' filters are used. These four filters combined offer a view from near infrared to near ultraviolet.

The objects chosen also need to be visible during certain time period for LCO 0.4m telescopes. LCO visibility calculator was used to determined visibility.[18]

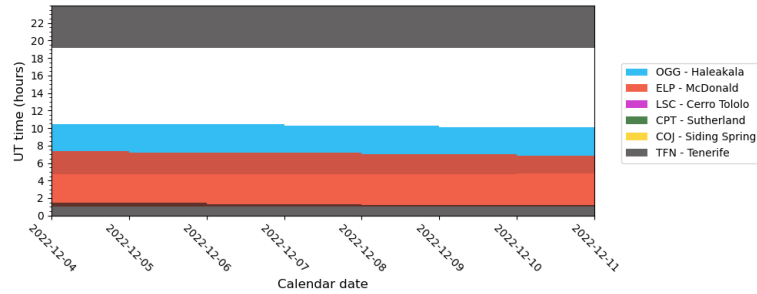


Рис. 2: One example observation window from 2022-12-04 to 2022-12-11 of BI CAS. The observation window for other targets can be found in the same way.

The integration time is calculated using LCO exposure and SNR calculator.[19]. A proper integration time is chosen so that CCD won't be saturated

Таблица I: observation parameter. Period data comes from [17]

Target Name	RA (J2000)	Dec (J2000)	Filter	# Exposures	Integration Time (s)	Observational Windows
ASASSN-V J004331.19+623955.9 / BI Cas	10.880	62.666	SDSS u'	3	120	Period: 1.099 day. 10 observations in 2 days
ASASSN-V J004331.19+623955.9 / BI Cas	10.880	62.666	SDSS g'	3	120	Period: 1.099 day. 10 observations in 2 days
ASASSN-V J004331.19+623955.9 / BI Cas	10.880	62.666	SDSS r'	3	120	Period: 1.099 day. 10 observations in 2 days
ASASSN-V J004331.19+623955.9 / BI Cas	10.880	62.666	SDSS i'	3	120	Period: 1.099 day. 10 observations in 2 days
ASASSN-V J004331.19+623955.9 / BI Cas	128.550	-68.600	SDSS u'	3	50	Period: 0.894 days. 10 observations in a day
ASASSN-V J083412.06-683601.2 / NSV 4148	128.550	-68.600	SDSS g'	3	50	Period: 0.894 days. 10 observations in a day
ASASSN-V J083412.06-683601.2 / NSV 4148	128.550	-68.600	SDSS r'	3	50	Period: 0.894 days. 10 observations in a day
ASASSN-V J083412.06-683601.2 / NSV 4148	128.550	-68.600	SDSS i'	3	50	Period: 0.894 days. 10 observations in a day
RR Lyrae	19 25 27.913	+42 47 03.694	SDSS u'	3	1	Period: 0.567 day 10 observations in a day
RR Lyrae	19 25 27.913	+42 47 03.694	SDSS g'	3	1	Period: 0.567 day 10 observations in a day
RR Lyrae	19 25 27.913	+42 47 03.694	SDSS r'	3	1	Period: 0.567 day 10 observations in a day
RR Lyrae	19 25 27.913	+42 47 03.694	SDSS i'	3	1	Period: 0.567 day 10 observations in a day

C. photometry

The data from the 0.4m telescope is pre-processed by the LCO BANZAI pipeline.[8] The data from the telescope was then imported into python using astropy package for further analysis. First the pictures taken under the same filter are sorted out. Calibration techniques is used to measure the apparent magnitude of the variable stars. Calibration is conducted using nearby stars in the field of view and the background sky. The light curve under different filters is then plotted. Pictures taken under different filters allow us to observe the varying magnitude under different wavelength. Compare the observed period-luminosity relation to other result. Period luminosity for classical Cepheid variables is

$$M_v = (-2.43 \pm 0.12)(\log_{10} P - 1) - (4.05 \pm 0.02)$$

given by Hubble Space Telescope trigonometric parallaxes for 10 nearby Cepheids.[15] The following relations can then be used to calculate the distance d to classical Cepheids

$$5 \log_{10} d = V + 3.34 \log_{10} P - 2.45(V - I) + 10.52[15]$$

or

$$5 \log_{10} d = V + 3.34 \log_{10} P - 2.55(V - I) + 10.48[16]$$

I and V represent near infrared and visual apparent mean magnitudes. The distance d is given in parsecs. The period-luminosity relation for type II Cepheid variables is given by

$$M = -0.35 - 1.75 \log P$$

Astro art is used to find the calibration star. In order to make more precise photometric measurement, it is better to choose brighter reference star to maximize signal-to-noise ratio. Coordinates of the reference stars were then input into the database to search for their magnitude. The information of the reference stars comes from SIMBAD[11]. Note that since a multi-band photometry was conducted, it is important to use magnitude data from different bands. Since the magnitude of a star may vary on different wave band, using a reference magnitude for all bands may result in discrepancy. Some of the stars in the SIMBAD database have magnitude measured in sdss u g r i filters. The images taken from the telescope is processed using python. Astropy and photutils packages are used to conduct photometry. First the images is sorted according their filter information. The Findstar function from photutils packages is used to locate stars and measure their flux on the image. The functions works based on such mechanism: The function locates pixel points that deviate from the background signal by a certain amount of standard deviation. This threshold can be customized. In practice, I set the threshold to be over 150σ . The function also excludes pixel points that have a full-width-at-half-maximum lower than some threshold to prevent locating hot pixels. I set the threshold to be 3 standard deviation

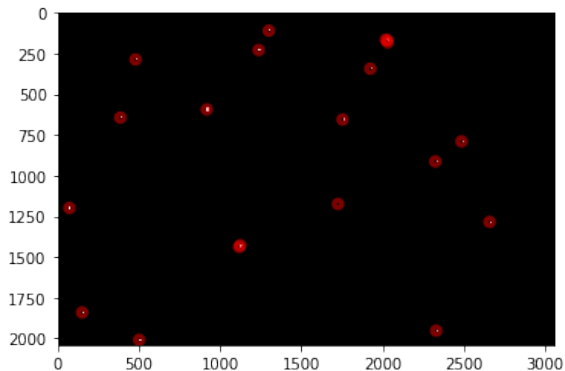


Рис. 3: The program finds out 20 brightest stars in the image taken for RR Lyrae.

D. period and frequency analysis

After plotting the calibrated magnitude, a special technique is used to find out the period of the variables. The Lomb-Scargle periodogram is a commonly used statistical tool designed to detect periodic signals in unevenly spaced observations.[12] It can be conveniently applied to our data using the LombScargle class in Astrpy package. Since the data obtained from the observation is unevenly spaced, it becomes the perfect tool that can be applied in the analysis of the data.

The Lomb-Scargle technique utilizes Fourier Transform, which is a useful tool in signal analysis and processing. Fourier transform of a continuous signal $f(t)$ is given by the integral [14]

$$F(f) = \int_{-\infty}^{\infty} g(t)e^{-2\pi ift} dt$$

This transformation transforms a signal in time domain to frequency domain. For Convenience the Fourier transform is usually denoted by operator \mathcal{F} . Such that the Fourier transform and the inverse Fourier transform can be denoted as

$$F(f) = \mathcal{F}(g(t))$$

and for the inverse Fourier transform

$$g(t) = \mathcal{F}^{-1}$$

However, in real world, there is only discrete data points but not continuous function. In this case, discrete Fourier transform, usually denoted as DFT, is used.

$$F(f) = \sum_{-\infty}^{\infty} g(n\Delta t)e^{-2\pi ifn\Delta t}$$

In this case, a continuous variable is substituted by a small block $n\Delta t$. The Fourier Transform gives a power spectrum density, known as PSD for a set of data. From the PSD of the data, the periodic behaviour and the frequency can be read out.

Lomb-Scargle method then use least square method to fit the data to a periodic model with three parameters

$$y(t, f, \theta) = \theta_0 + \sum_{n=1}^{nterms} [\theta_{2n-1} \sin(2\pi nft) + \theta_{2n} \cos(2\pi nft)]$$

E. error analysis and calibration

The magnitude measured for the reference stars chosen may not be the same for each images. However, the reference stars chosen are not variable stars, The reasons that may explain this phenomenon are probably the background noise of the night sky and the CCD may be in different configuration each time. Thus a normalizing constant has to be introduced to normalized the magnitude of the three reference star to the same magnitude as they are in the first image. The normalizing constant is given by the equation

$$n = \frac{M_1}{M_i}$$

The calibrated magnitude is normalized by the normalizing constant

$$M_{calibrated} = n * (M_{raw} - M_{zp})$$

The error in measuring is given by the equation

$$\delta M_{calibrated} = M_{calibrated} * \sqrt{\left(\frac{\delta n}{n}\right)^2 + \left(\frac{\sqrt{\delta M_{raw}^2 + \delta M_{zp}^2}}{M_{raw} - M_{zp}}\right)^2}$$

M_{raw} stands for the magnitude before calibration, which is adding the zero point offset. The uncertainty δn and δM_{raw} can be calculated using the standard deviation of these data.

III. ANALYSIS

A. RR Lyrae

Plot out the raw data measured from the aperture sum of the images of RR Lyrae

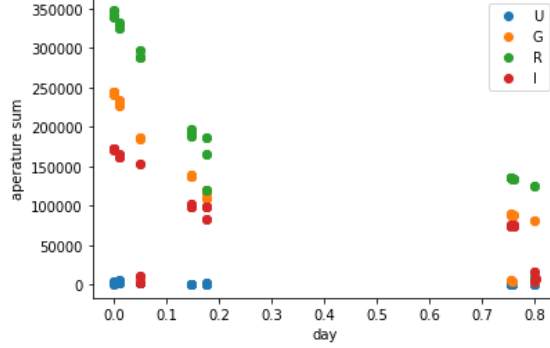


Рис. 4: The raw data, measuring the aperture sum, from the observation of RR Lyrae under different filters. A significant variation can be seen in the graph.

The magnitude of a star is calculated using

$$m = -2.5 \log_{10}(N_{\text{aperture sum}})$$

before calibration The magnitude after calibration is calculated using

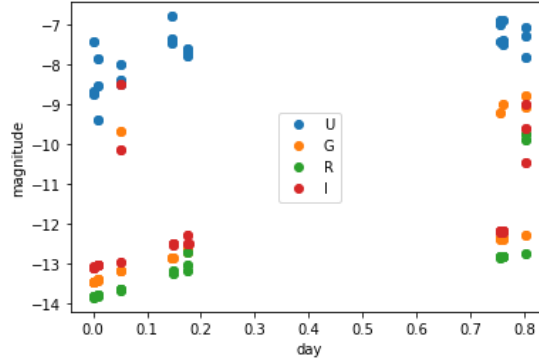


Рис. 5: Plot the data using magnitude before calibration

$$m_{\text{calibrated}} = m + ZP$$

Where ZP is the zero point difference. When doing photometry, we note that the photos taken under sdss u filter has very low quality. On the photos taken under the u filter, only RR lyrae can be barely recognized. Other stars which can be used as reference star can be hardly recognized. As a result, calibration can not be done for images taken under u filter. It seems like the stars themselves are too dark on ultraviolet band. For the calibration process below, we use only images taken under g r and i filters, neglecting the images taken under the ultraviolet band. From the picture it can be seen that the image taken under sdss U filter is too bad to conduct analysis.

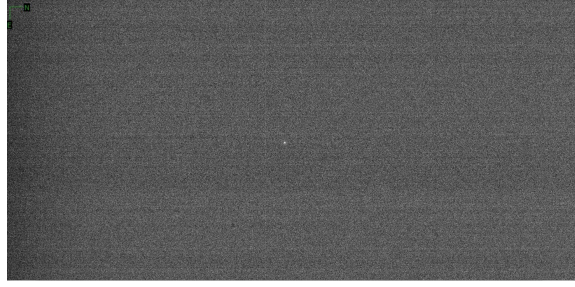


Рис. 6: The image taken under filter u. Only RR lyrae can be barely recognized



Рис. 7: Locate the reference stars using astroart. This image is taken under the sdss r filter.

Choosing these three stars as the reference star. The data comes from SIMBAD database[11]. They are chosen because they are relatively bright and have a complete magnitude data measured under sdss g r and i filter.

Таблица II: reference star parameters for RR Lyrae[11]

Reference stars name	RA coordinate	DEC coordinate	g filter magnitude	r filter magnitude	i filter magnitude
UCAC4 663-075895	19 25 31.6321974576	+42 34 49.029074832	12.991±0.05	12.170±0.04	11.861±0.02
UCAC4 664-074538	19 25 17.1222077784	+42 37 01.642304496	13.099±0.04	12.432±0.03	12.153±0.03
UCAC4 663-076028	19 26 09.7910026752	+42 34 24.371817276	13.624±0.03	13.270±0.04	13.157±0.03

Plotting the magnitude of RR lyrae after calibration through time.

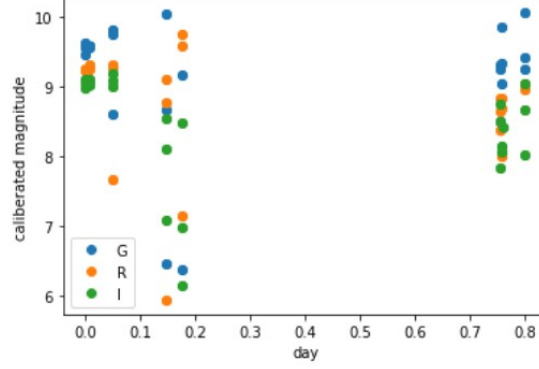


Рис. 8: The magnitude of RR Lyrae after using the three calibration star.

Separate the data point under different filter band can plot them into different graphs.

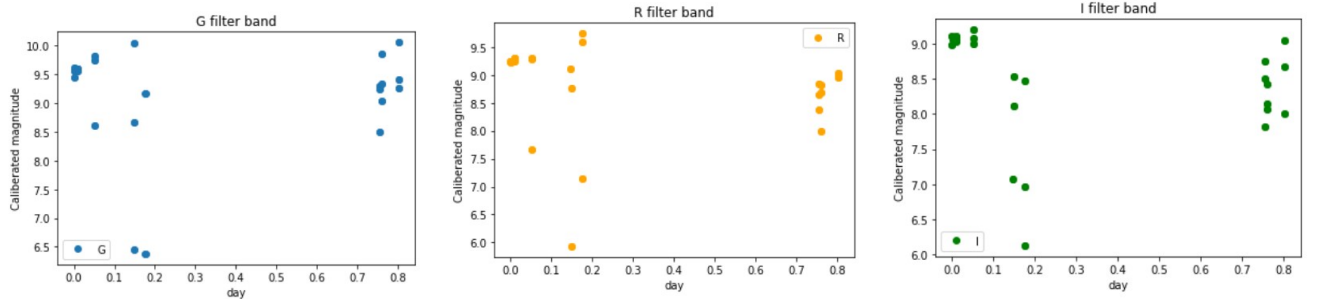


Рис. 9: The magnitude of RR Lyrae under G, R, and I filter band, respectively

Plotting the magnitude of the calibration stars calculated directly from the images.

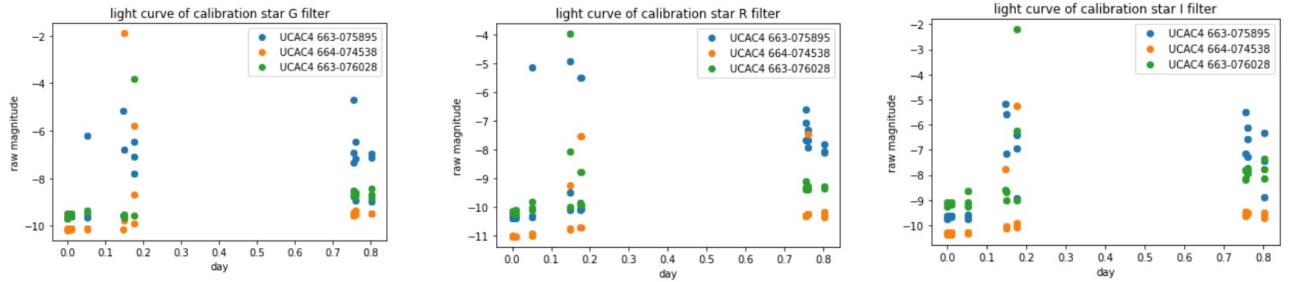


Рис. 10: the magnitude of the calibration stars calculated directly from the images.

We can see from the figure that the magnitudes of the calibration stars are generally stable from image to image. However there are still some outliers

Next step is calculating the normalizing constant and its uncertainties. In case of there are three reference stars here, we calculate the normalizing constant of one particular image for each of the stars and take the average of the three numbers as the normalizing constant for this image. To calculate the uncertainty of the normalizing constant

δn , the standard deviation of the normalizing constants for all of the three stars is taken. Thus, the normalizing constant and the uncertainty of the normalizing constant for each image is determined.

The uncertainty provided in the data base for the magnitude of the reference stars is used as δM_{zp} . The uncertainty can be looked up in table II. Since three reference stars were chosen, the average of the uncertainty of the magnitude of the three reference stars is taken as δM_{zp} .

To calculate δM_{raw} , the error propagating feature in `photutils.aperture_photometry` is used. To use this feature, we need to first input an array of error for each of the pixel points in the image. After that, the function will propagate the error value use

$$\Delta F = \sqrt{\sum_{i \in A} \sigma_{tot,i}^2}$$

Where A are the non-masked pixels in the aperture and $\sigma_{tot,i}$ is the input error array.[13] In this case we take error to be 0.015 times the pixel value. The 0.015 time value corresponds to a signal to noise ratio of approximately 70. This value is the upper bond of the uncertainty. Measuring the signal to noise ratio of the three reference stars using `astro art`, I found that they both have a signal to noise ratio higher than 70. The uncertainty value given by this process is the uncertainty in the flux measured from the image. This uncertainty needed to be converted into uncertainty in magnitude. However, logarithm is not linear, so the average of both the change in magnitude in the positive direction and in the negative direction is taken to be δM_{raw} . It is expressed by the equation

$$\delta M_{raw} = -2.5 * \frac{1}{2} (\lg(\frac{N_{aperatruesum} + \delta N}{N_{aperatruesum}}) + \lg(\frac{N_{aperatruesum}}{N_{aperatruesum} - \delta N}))$$

Calculating the uncertainty using the above equations and plot out error bars.

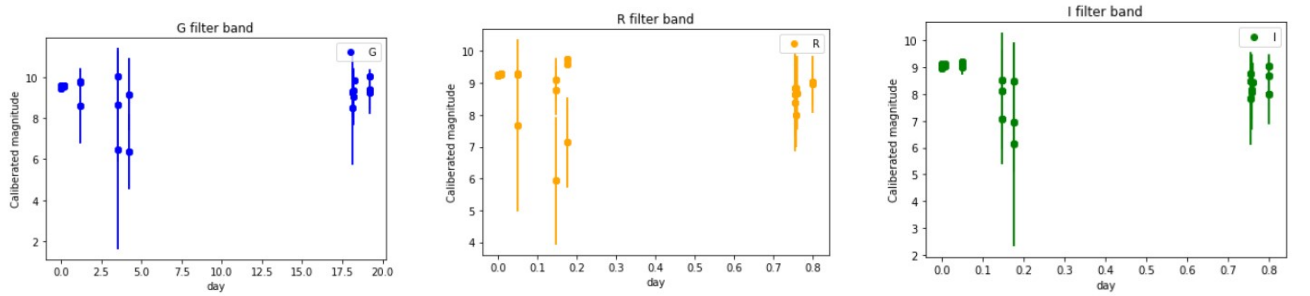


Рис. 11: The calibrated magnitude for RR Lyrae with error bars plotted

Note that in these figures, the outlier values has longer error bars, indicating that systematic errors may occur. Using the Lomb-Scargle method to analyze the frequency of the RR Lyrae variable star and then draw out the power spectrum density diagram.

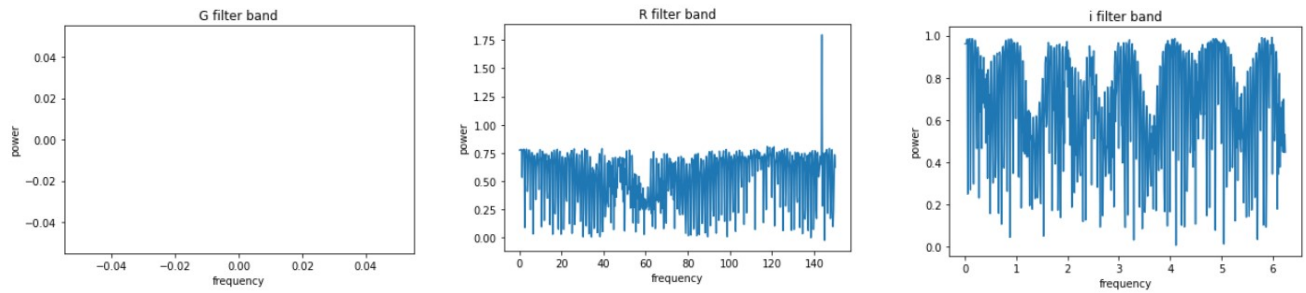


Рис. 12: The power spectrum density after using Lomb-Scargle method to analyze the data with uncertainty under g r and i band for RR Lyrae

However, due to some build-in error or limitations of the function `lomb-Scargle.autopower()`. The power spectrum density for the data under G band is not successfully drawn out. After checking the program, we found out that the frequency data points returned by this function when inputting G filter data are all none type variables. I failed to solve this problem so only analyses for r filter data and i filter data are done below. Find out the maximum and the standard deviation of the frequency data

Таблица III: results of the r and i filter power spectrum density for RR Lyrae

	R filter	I filter
Most probable frequency	149.882 day ⁻¹	43.3032 day ⁻¹
Standard deviation	6.243	1.8038

Using the best fit parameters calculated by the LombScargle function. Plot out the model which the data is fitted to and adjust the position of the data points to be in phase of the model

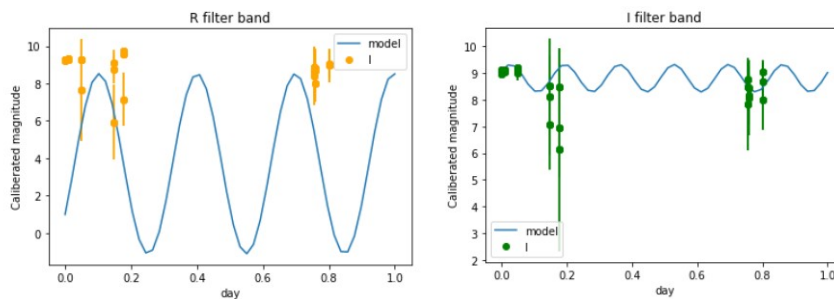


Рис. 13: Plot the model together with the data for RR Lyrae

B. BI Cas

For the star BI Cas, which is a classical type Cepheid variable, similar process is conducted. This time, choosing the reference stars to be Note that this time the object star is not the brightest star in the field. As a result, first

Таблица IV: reference star parameter for BI Cas[11]

Reference stars name	RA coordinate	DEC coordinate	g filter magnitude	r filter magnitude	i filter magnitude
HD 3949	00 42 48.5115495240	+62 45 57.097433448	7.763291 \pm 0.00277	7.79 \pm 0.03	7.79 \pm 0.42
UCAC4 764-009281	00 43 54.3609383483	+62 44 29.58664229	12.260 \pm 0.02	11.807 \pm 0.03	11.639 \pm 0.04
UCAC4 764-009265	00 43 41.9666592251	+62 45 53.367092577	14.122 \pm 0.03	13.0050 \pm 02	12.490 \pm 0.04

I need to modify the python functions that were previously defined to do the photometry for RR Lyrae. Since RR Lyrae is the brightest star in the field, to locate RR Lyrae, Locating RR Lyrae only needs to locate the brightest pixel point. However, that is not the case for BI Cas. The stars that is closest to the center of the field need to be located. Also Note that for HD 3949, there is no Sloan Digital Sky Survey data for this star. As a result, its magnitude is not measured under sdss u' g' r' i' filter. Instead, GAIA data is used. GAIA data only provides magnitude measured under B, V,G,J,H,K filters. Among then, filter G can be consider approximately the same as sdss g' filter. The magnitude measured under V filter is used as r filter magnitude and i filter magnitude. The difference between G and V magnitude is used as the uncertainty in g filter magnitude. Similarly, the difference between J and V filter is used the uncertainty in i filter magnitude



Рис. 14: Locate the reference stars and the object stars using astroart. This image is taken under the sdss g filter.

Again we neglect the images taken under filter u' because of their low signal to noise ratio. It is very hard to recognize our reference stars and object star on such images.

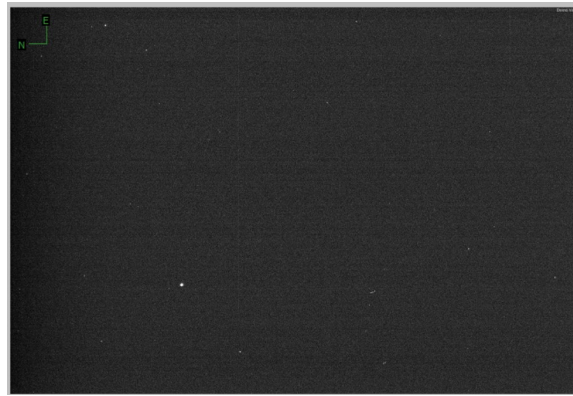


Рис. 15: The image taken under filter u. Only the brightest star, HD 3949 can be barely recognized.

plotting out the light curve of the calibration stars for BI Cas

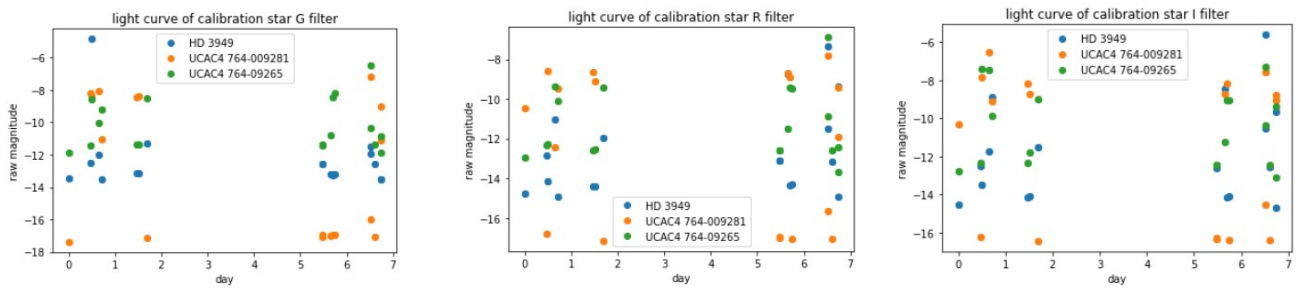


Рис. 16: the magnitude of the calibration stars calculated directly from the images.

Note that from the image it can be concluded that the measured flux of the reference stars is not always constant. There are also some outliers. As a result, it is necessary to do normalization.

Plot out the normalized light curve of the reference stars.

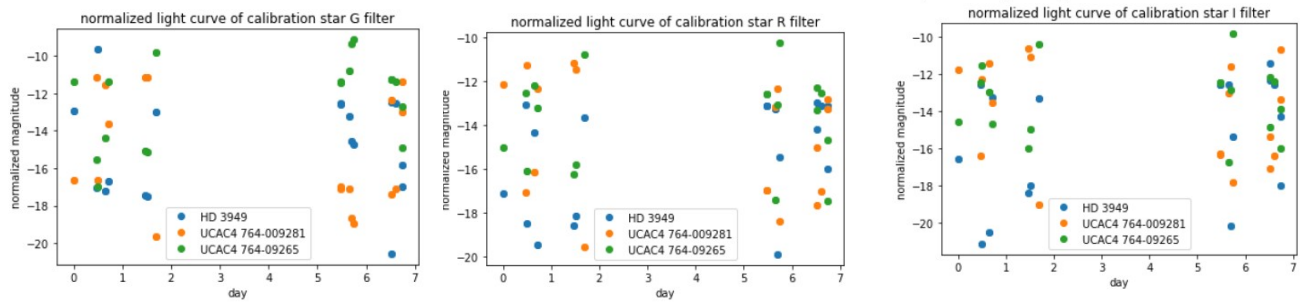


Рис. 17: the normalized magnitude of the calibration stars .

Plot out the calibrated magnitude through time of BI Cas as below

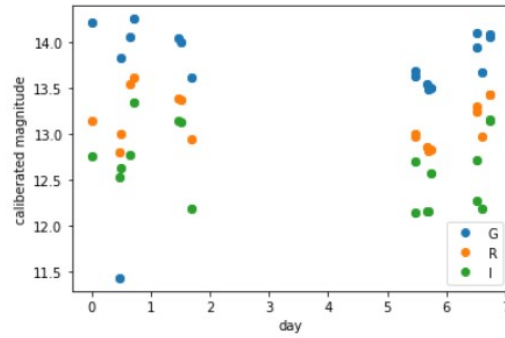


Рис. 18: The calibrated but unnormalized magnitude of BI Cas

Normalized the magnitude data and add in error bars. Plot different filter data respectively

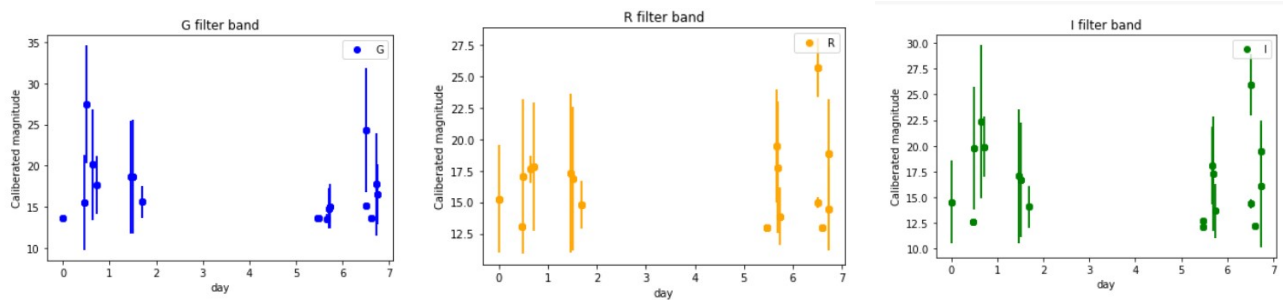


Рис. 19: The normalized magnitude-time data of BI Cas under g, r and i filters, with error bars plotted.

Utilizing Lomb-Scargle method, obtain the power density spectrum for the data

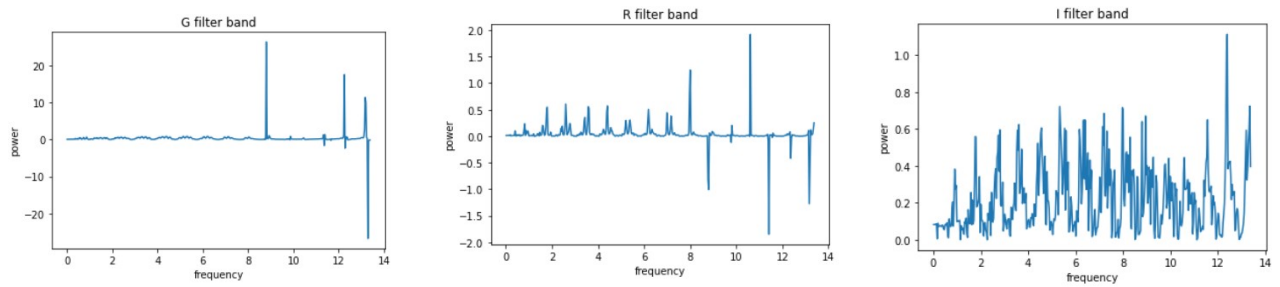


Рис. 20: The PSD for the magnitude-time data under g, r and i filters for Bi Cas.

Plotting out the best fit model that Lomb-Scargle method fits to, and adjust the x location of the data points to plot it in phase with the model

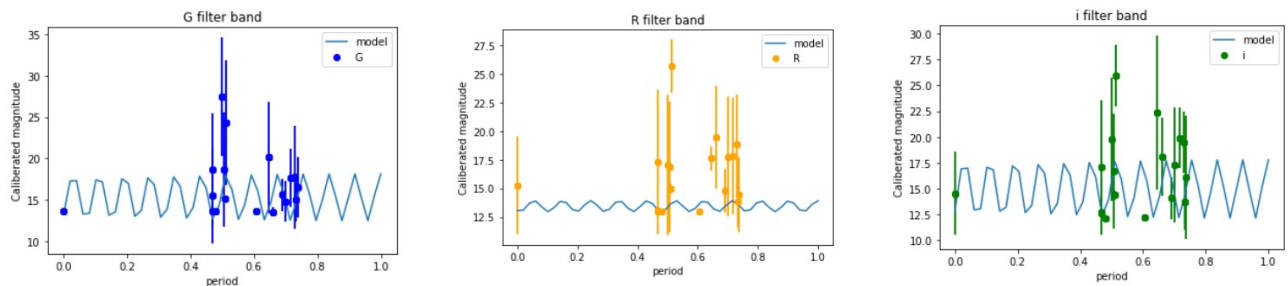


Рис. 21: The phase data of Bi Cas.

Таблица V: Frequency and uncertainty of BI Cas

	G filter	R filter	I filter
Most probable frequency	8.801682 day ⁻¹	10.6128 day ⁻¹	13.3734 day ⁻¹
Standard deviation	3.8648	3.8649	3.865

This is the frequency given by the Lomb-Scargle method.

IV. RESULTS

A. conclusion

In this paper, we measured the magnitude to light relations for two Cepheid variable stars, RR Lyrae and BI Cas. RR Lyrae is classified as anomalous Cepheid variable and BI Cas is classified as classical Cepheid variable. Calibration stars from the field of view are chosen to calibrate the magnitude. Normalization technique is also used to offset the difference from image to image. Finally, Lomb-Scargle method is used to obtain the power spectrum density and fit the data to a periodic model. Lomb-Scargle method gives the most probable frequency for the data sampled with an uneven time spacing from a periodic source.

By observing the calibrated and normalized magnitude figures that were drawn, some conclusions can be drawn. Many of the magnitude of our measurements are close to the mean magnitude that is given by the database. However, there are also some outliers, but these outliers all have very long error bars, which suggest that the outlying values may not be very far from the mean magnitude. We can conclude that a good job of error analysis is done. The power spectrum density figures that were drawn suggest that there is not noticeably outstanding frequency. The reason why is explained below

B. Comparison

Look up the result given in other data base and compare those result with our data. From the ASAS-SN data base,[17] the period of Bi Cas is given by 1.099287day , which correspond to a frequency of 0.91day^{-1} . The result given by ASAS-SN is very far from the measurement and analysis that was done above. The frequency obtained ranging from 8.801682day^{-1} to 13.3734day^{-1} For magnitude measured under G filter and I filter. The period for Bi Cas given from the database is over 3σ over from my measurement and analysis.

The period of RR Lyrae is not provided by asas-sn database. It is given by Kolenberg, K.; et al. (February 2011) [20] as 0.56686776 days (13 hours, 36 minutes), which in terms of period, is 1.764day^{-1} . Obviously my analysis result for the period of RR Lyrae is also far from this value. The discrepancy is larger then 3σ There must be some problems associate with the measurement or analysis above. Many reasons can be attributed to this phenomenon.

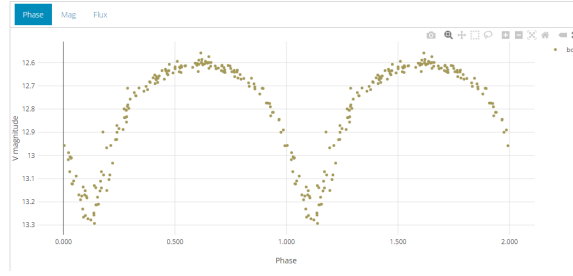


FIG. 22: The phase diagram of BI Cas given by ASAS-SN.

In the asas-sn database, the phase diagram and the period of RR Lyrae are both not provided, so I download the magnitude data from asas-sn database and try to do some analysis myself.[17]

The magnitude data from asas-sn[17] is provided in three columns, which are time, magnitude, and error in magnitude. There are also two types of data, magnitude measured using bb camera and magnitude measured using ba camera. Only bb data is used in this case. First plot out the magnitude versus time figure.

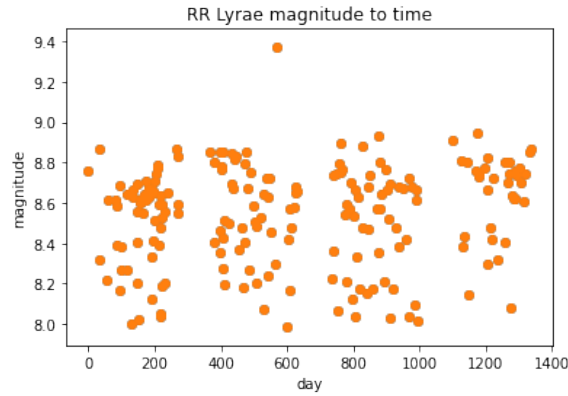


FIG. 23: The magnitude-time figure plotted using data from asas-sn

This set of data contains 198 samples. Note that the samples have larger amount and are distributed more evenly through time then our measurement. It can be noted that though the data is also made up of several sampling period

separated by time gaps, the gaps are relatively shorter than the overall sampling time. Error bars at a length of 0.02 magnitude are also plotted, but they are too small to be viewed on the figure

Similarly, Lomb-Scargle method is used to analyze the data. Note that the PSD of this set of data contains several

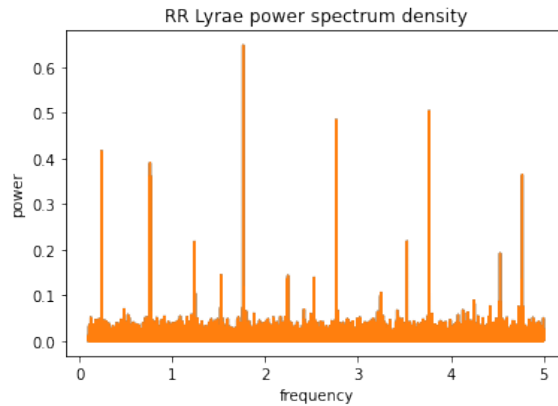


Рис. 24: The power spectrum density figure of the data

spikes. It is necessary to adjust the frequency range of the Lomb-Scargle function in order to convey the interested frequency band.

It can be concluded from the PSD that the most probable frequency is

$$1.7643273297635784 \text{ day}^{-1}$$

with a standard deviation

$$\sigma = 1.4145106233476583$$

The result is very close to the cited period of RR Lyrae above, within one standard deviation. It can be concluded that Lomb-Scargle method can work well if more sampling points with more even distribution through time can be provided.

Plot out the phase diagram of RR Lyrae data with the best fit model provided by Lomb-Scargle method

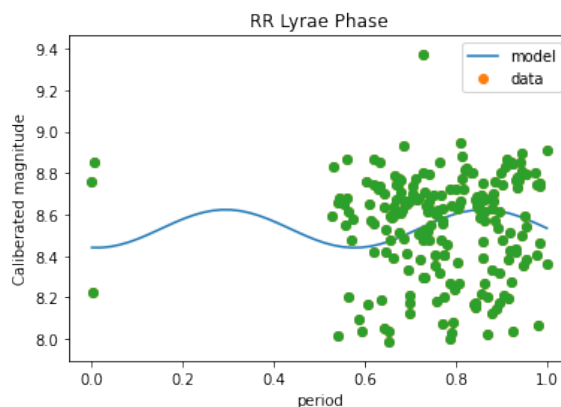


Рис. 25: The data and the best fit model provided by Lomb-Scargle method

Note that the sampling points are not distributed evenly in phase. This may explain why the most probable frequency only has a power 0.64796. If the sampling points are distributed more evenly in phase, a better light curve may be drawn.

Compare this model to the light curve of RR Lyrae drawn by others

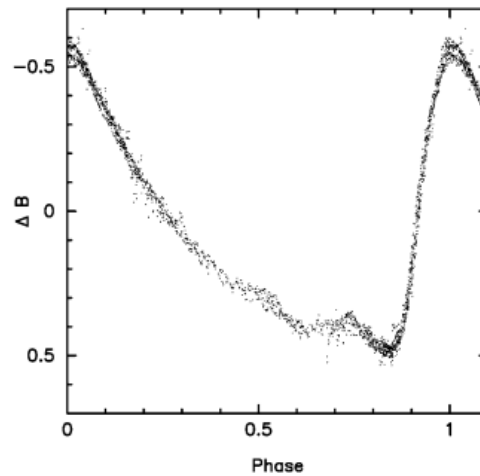


FIG. 5.—*B* light curve of RR Lyrae, with the sidelobes of the frequency triplets removed.

Рис. 26: B band light curve of RR Lyrae, with the sidelobes of the frequency triplets removed. Cited from[22]

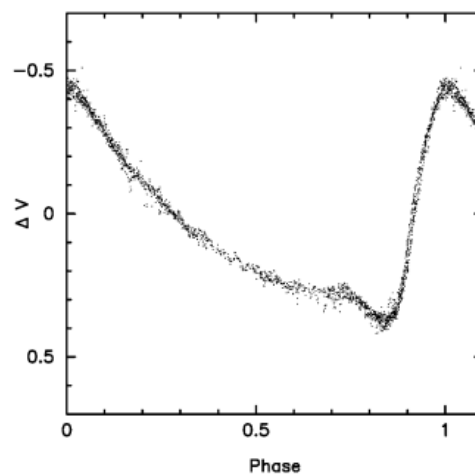


Рис. 27: V band light curve of RR Lyrae, with the sidelobes of the frequency triplets removed. Cited from[22]

Note that RR Lyrae exhibits different light curve when it is measured under different filter band. Also note that The light curves were plotted with the sidelobes of the frequency triplets removed. Only in this way the light curves can have such a neat shape. Usually the light curves can be a combination of two or more frequencies. This information can be read out in the PSD. The dominant frequency is chosen to be the frequency of the variable stars. There are also Cepheid variables that have been observed to pulsate in two modes at the same time.[23]

V. DISCUSSION

A. Limitation and possible improvement

Some reasons can explain the large discrepancy between our measurement and the data provided from the database. First, the sampling rate is too low and the samples are too far from each other. For more optimal use of Lomb-Scargle method, longer sampling time and larger amount of samples is needed. The amount of samples is limited by the observational window. The telescope time that was provided is very limited, we can only take some samples within a relatively short period of time compared to the period of the Cepheid Variables. The time difference between two period of time that we can take samples is large. As a result, this limitation prevented us from obtaining the data for a complete cycle. We are always observing the same phase in the period of the Cepheid variable stars. The large time gap between two sampling period results in a bad fit to the model when conducting Lomb-Scargle analysis. If we can obtain larger samples over a longer sampling period and if the samples are distributed relatively more even than over data, Lomb-Scargle method may give a closer frequency and a better model.

Second, the sdss u, g, r, and i filters are not perfectly same with V and G filters, resulting in some error in the magnitude of the reference stars that were chosen. However, five of the six reference stars that were chosen have magnitude data that is measured under sdss u'g'r' and i filters. The only one reference star that does not have sdss data is HD3949. This error may only have minor contribution to the final result since the discrepancy itself is not significant and magnitude data is averaged with other more precise magnitude data, significantly reducing the contribution. If possible, images under more filters but not just the sdss filters can be taken in order to provide broader insight to the research problem.

Third, The method I used to locating stars is by running a python program that involves using functions in astropy and photutils packages. However, the star finding function is somehow too sensitive even if I set the sigma to over 1500 and can not distinguished stars from other noise or hot pixels very well. When designing the program, I tuned the program so that it located stars based on the following mechanism: The program will first find the position of all the stars on a image and compare the distance from each stars to the star coordinates I input. It will then choose out all the stars within a certain distance to the coordinates and use the largest flux among these stars as the flux of the star I am finding. In practice, I set the threshold to be 100 pixels. This mechanism is supposed to work well since the stars I chosen are all relatively bright and any star is brighter than them which is within 100-pixel-distance can be hardly found. However, In practice I also noticed that sometimes the star coordinate that was located using the program was over 60 to 80 pixels away from the coordinate I input. As a result, I am not entirely sure that the star which the program locates is the same as what I suppose it to be. This reason may results in the outliers in the magnitude of the reference stars and thus abnormal normalizing constant. It can explain why some outlier points have very long error bars. Since a wrong star is located, the normalizing constant for this star is greatly different from those of the other two stars, resulting in big standard deviation and thus large δn . Better star finding functions which are able to eliminate noise can give more reliable star finding results. Additionally, if possible, package from astrometry.net[21] can also be utilized. This package can locate stars precisely using their relative positions. API ports to star database may also be used to look up the data for reference stars atomically and can effectively reduces workload.

Forth, in this experiment, the images taken under sdss u' filters are all discarded because of low quality, failing to

provide any insight for the light variation of variable stars on ultraviolet band, since most of the objects on the image can not be effectively identified. The reason for this result may be attributed to the low magnitude on ultraviolet band of most of the stars when observing on earth. This is because the Earth's atmosphere blocks most of the ultraviolet light. The images taken under ultraviolet band requires longer exposure time. To improve this, we may have to customize observing parameters for different filters

VI. ACKNOWLEDGEMENTS

This work makes use of observations from the Las Cumbres Observatory global telescope network. This paper is based on observations made with the SBIG 6303 0.4-meter telescope, McDonald Observatory, Fort Davis, Texas, operated by the Las Cumbres Observatory

This work makes use of data from ASAS-SN and simbad database

Thank you for helping provided by PHYS 134L Professor Lubin and TA Kim.

Thank you for cooperation by group mates Shihao Zhou and Vincent Wei.

VII. REFERENCE

- [1] ASAS-SN Variable Stars Database <https://asas-sn.osu.edu/variables>
- [2] Leavitt, Henrietta S. (1908). "1777 variables in the Magellanic Clouds". *Annals of the Astronomical Observatory of Harvard College*. 60 (4): 87–108.
- [3] Leavitt, Henrietta S.; Pickering, Edward C. (1912). "Periods of 25 variable stars in the Small Magellanic Cloud". *Harvard College Observatory Circular*. 173: 1–3.
- [4] Hubble, E. P. (1925). "Cepheids in spiral nebulae". *The Observatory*. 48: 139.
- [5] LCO instruments <https://lco.global/observatory/telescopes/0m4/>
- [6] LCO exposure time calculator <https://exposure-time-calculator.lco.global/>
- [7] LCO filter transmission graph <https://lco.global/observatory/instruments/filters/sdss-r/>
- [8] LCO BANZAI pipeline <https://lco.global/documentation/data/BANZAIpipeline/>
- [9] Eddington, A. S. (1917). "The pulsation theory of Cepheid variables". *The Observatory*. 40: 290.
- [10] Zhevakin, S. A. (1953). "К Теории Цефеид. I". *Астрономический журнал*. 30: 161–179.
- [11] SIMBAD database <http://simbad.cds.unistra.fr/simbad/sim-fcoo>
- [12] astropy package documentation <https://docs.astropy.org/en/stable/timeseries/lombscargle.html?highlight=period>
- [13] photutils package documentation <https://photutils.readthedocs.io/en/stable/aperture.html?highlight=noiseaperture-photometry-error-estimation>
- [14] VanderPlas, J. Understanding the Lomb-Scargle Periodogram *ApJS* 236.1:16 (2018) <https://ui.adsabs.harvard.edu/abs/2018ApJS..236...16V>
- [15] Benedict, G. Fritz; McArthur, Barbara E.; Feast, Michael W.; Barnes, Thomas G.; Harrison, Thomas E.; Patterson, Richard J.; Menzies, John W.; Bean, Jacob L.; Freedman, Wendy L. (2007). "Hubble Space Telescope Fine Guidance Sensor Parallaxes of Galactic Cepheid Variable Stars: Period-Luminosity Relations". *The Astronomical Journal*. 133 (4): 1810. arXiv:astro-ph/0612465. Bibcode:2007AJ....133.1810B. doi:10.1086/511980.
- [16] Majaess, Daniel; Turner, David; Moni Bidin, Christian; Mauro, Francesco; Geisler, Douglas; Gieren, Wolfgang; Minniti, Dante; Chené, André-Nicolas; Lucas, Philip; Borissova, Jura; Kurtev, Radostn; Dékány, Istvan; Saito, Roberto K. (2011). "New Evidence Supporting Membership for TW Nor in Lyngå 6 and the Centaurus Spiral Arm". *The Astrophysical Journal Letters*. 741 (2): L27. arXiv:1110.0830. Bibcode:2011ApJ...741L..27M. doi:10.1088/2041-8205/741/2/L27. S2CID 12220317.
- [17] ASAS-SN variable database <https://asas-sn.osu.edu/variables/>
- [18] LCO visibility calculator <https://lco.global/observatory/visibility/>
- [19] LCO Exposure and SNR calculator exposure-time-calculator.lco.global/
- [20] Kolenberg, K.; et al. (February 2011), "Kepler photometry of the prototypical Blazhko star RR Lyr: an old friend seen in a new light *Monthly Notices of the Royal Astronomical Society*, 411 (2): 878–890, arXiv:1011.5908, Bibcode:2011MNRAS.411..878K, doi:10.1111/j.1365-2966.2010.17728.x, S2CID 73597094
- [21] Astrometry package website <https://astrometry.net/>
- [22] The Blazhko Effect of RR Lyrae in 1996 Horace A. Smith et al 2003 *PASP* 115 43
- [23] Soszynski, I.; Poleski, R.; Udalski, A.; Kubiak, M.; Szymanski, M. K.; Pietrzynski, G.; Wyrzykowski, L.; Szewczyk, O.; Ulaczyk, K. (2008). "The Optical Gravitational Lensing Experiment. Triple-Mode and 10/30 Double-Mode Cepheids in the Large Magellanic Cloud". *Acta Astronomica*. 58: 153. arXiv:0807.4182. Bibcode:2008AcA....58..153S.